ACS Catalysis

Letter

pubs.acs.org/acscatalysis

Cavity Controls the Selectivity: Insights of Confinement Effects on MTO Reaction

Jinzhe Li,[†] Yingxu Wei,[†] Jingrun Chen,[†,§] Shutao Xu,[†] Peng Tian,[†] Xiaofeng Yang,[‡] Bing Li,[†] Jinbang Wang,[†,§] and Zhongmin Liu*[,†,‡]

[†]National Engineering Laboratory for Methanol to Olefins, Dalian National Laboratory for Clean Energy, Dalian Institute of Chemical Physics, Chinese Academy of Sciences, Dalian 116023, China

[‡]State Key Laboratory of Catalysis, Dalian Institute of Chemical Physics, Chinese Academy of Sciences, Dalian 116023, China

[§]Graduate University of Chinese Academy of Sciences, Beijing 100049, China

Supporting Information

ABSTRACT: Organic reaction intermediates confined in zeolite cavities are very important for product formation during methanol-to-olefins (MTO) conversion; however, direct evidence is still required to understand the particular function of these intermediates. Herein, for the first time, by careful selection of SAPO molecular sieves with different cavity size but identical 8MR pore openings, the reactivity and role of these intermediates played in olefin generation are verified by isotopic tracing method and theoretical calculations based on the observation of two types of carbenium intermediates, polyMB$^+$ and polyMCP$^+$, under the real MTO reaction conditions. It demonstrates that cavity size controls the molecular size and reactivity of these confined species, which results in different MTO activity and product selectivity.

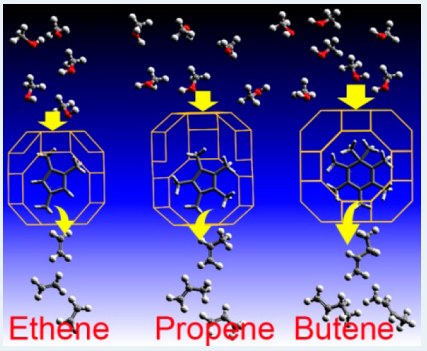

KEYWORDS: *MTO, C1 chemistry, shape selectivity, confinement effects, selectivity control*

Shape selectivity as the key feature of zeolites is one of the foundations of their wide utilization in catalysis and adsorption processes.[1,2] Methanol-to-olefins (MTO) reaction catalyzed by zeolite with shape-selective effects has attracted considerable attention in the field of C1 chemistry. In 2010, the world's first commercial MTO plant with a capability of 600 kt/y light olefins (ethene plus propene) was successfully put into stream in Baotou, China, in which the DMTO process developed by Dalian Institute of Chemical Physics has been adopted.[3] Currently, there are several commercial MTO processes developed by different research organizations or companies.[4] In parallel with MTO process development, great efforts have been devoted to a better understanding of the reaction mechanism which would be helpful for designing new efficient catalyst and promoting product selectivity.

The reaction mechanism of MTO conversion has been considered to be very complicated.[4−6] For example, although the molecules of reactant (methanol) and products (olefins) are small, larger reaction space (channel intersections and/or cavities) is generally required for the proper catalyst (e.g., SAPO-34 used in DMTO process).[5a,b] Researchers attributed this to the big intermediates appeared in olefin formation mechanisms.[6,7] Large aromatic-based intermediates confined in the cavities are considered responsible for converting methanol to olefins in the so-called "hydrocarbon pool" mechanism.[7a,b,8] In this connection, the cavity size and/or structure should play an essential role in the generation of these intermediates. Theoretical calculations suggest that the transition-state shape selectivity should govern the reaction with the participation of bulkier intermediates such as polymethylbenzenes.[7c] To the best of our knowledge, there is no direct evidence for the aforementioned speculation due to the difficulties in trapping and identifying the reaction intermediates in experiments.

In previous studies, we directly observed the heptamethylbenzenium cation (heptaMB$^+$) and pentamethylcyclopentadienium cation (pentaMCP$^+$) over DNL-6[7a] and SSZ-13[9] with particularly strong acidity during MTO reaction. However, the direct observation of carbenium cations over SAPO-34, the industrial catalyst with an eight-membered ring (8MR) used in the MTO process, is still a challenge. Furthermore, to understand the crucial role of zeolite cavities and the particular function of specific intermediate, the interplay of zeolite structures and confined species must be taken into account.

Herein, three silicoaluminophosphate (SAPO) molecular sieves (SAPO-35, SAPO-34, and DNL-6) with cavities and same 8MR pore openings (Scheme 1) are systematically chosen to directly compare the reactions in different cavities and to explore the confinement effects on the intermediates. For the first time, different types of polymethylbenzenium cation

Received: October 28, 2014
Revised: November 26, 2014
Published: December 19, 2014

DOI: 10.1021/cs501669k
ACS Catal. 2015, 5, 661−665

Scheme 1. Cavity Structures of 8MR Molecular Sieves: SAPO-35(Left, *lev* Cavity, 6.3 × 7.3 Å), SAPO-34(Middle, *cha* Cavity, 6.7 × 10 Å) and DNL-6 (Right, *α* Cavity, 11.4 × 11.4 Å)

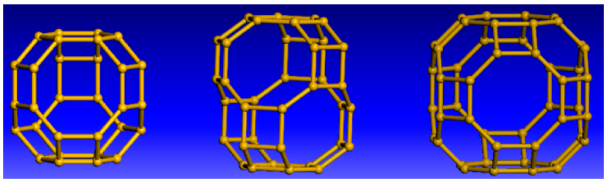

(polyMB$^+$) and polymethylcyclopentadienium cation (polyMCP$^+$) are directly observed over SAPO-35 and SAPO-34 under real MTO reaction conditions, whose molecular size and reactivity are different from those obtained over DNL-6. These findings supported by theoretical calculations evidence that the cavity size controls the reaction within the limited spaces which determines the type and reactivity of intermediates. To correlate these findings to their different catalytic performances, it is suggested that the cavity size also controls the MTO conversion and product distribution.

The as-prepared samples, SAPO-35, SAPO-34, and DNL-6, are well crystallized without impurity as seen from the SEM pictures (Figure S1) and the XRD patterns (Figure S2). The chemical compositions, N_2 adsorption−desorption isotherms, NH_3-TPD profiles, and ^{1}H MAS NMR spectra are shown in Table S1 and Figure S3,S4. The detailed ^{27}Al, ^{31}P, and ^{29}Si MAS NMR spectra of the calcined samples are shown in Figure S5−S7.

MTO results are shown in Figure 1. It is interesting that the maximum methanol conversion varies with the cavity size.

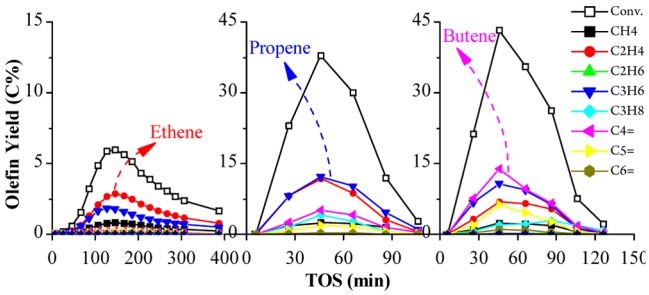

Figure 1. Conversion and olefin yields over SAPO-35 (left), SAPO-34 (middle), and DNL-6 (right) in MTO reaction at T = 275 °C, WHSV of methanol = 2.0 h^{-1}, He/methanol (mol) = 10.

SAPO-35 exhibits the lowest activity, and DNL-6 presents the highest activity. SAPO-34 possesses similar acidity as SAPO-35 (Figure S4), but the methanol conversion over SAPO-34 is much higher than that over SAPO-35. Apparently the difference in MTO performance for the three catalysts could not be simply explained by their difference in acidity, which implies the intrinsic reaction mechanism may vary with the cavity structure. On the other hand, the yields of olefin products also change with the cavity size. It is found that ethene and butenes are the predominant olefins over SAPO-35 and DNL-6, respectively, and propene and ethene show comparably importance in olefin products over SAPO-34. The similar trends are also found for different methanol conversions (as shown in Figure S8). Considering their same 8MR pore openings, one can deduce that some aspects related to cavity structure, rather than the product shape selectivity, govern the reaction.

To reveal the underlying mechanisms, in situ solid-state NMR and ex situ GC-MS studies are performed, which have been proven very powerful in identifying the active intermediates.[7a,8a−c,10] In this work, the measurements are carried out on the catalysts quenched at the time of maximum methanol conversion. The confined species measured with ^{13}C solid-state NMR are shown in Figure 2. The signals at 23.6−25 and 130−140 ppm in the spectra indicate the formation of alkylated aromatics, such as polymethylbenzenes.[11] The slight difference in chemical shift possibly results from the different number of the methyl groups on aromatics. The resonance peaks at 11, 28−30, 38, and 43−45 ppm can be assigned to carbon atoms from methyladamantanes.[10] The signals at 50 and 60 ppm represent the physisorbed methanol and dimethyl ether.[12] The signal at 56−57 ppm comes from surface methoxy groups on acid sites.[5d,12]

It is very interesting to observe the peaks at 242, 203, 195, and 154 ppm over SAPO-35; peaks at 244, 203, 190, 154, and 152 ppm over SAPO-34; and peaks at 243, 198, 188, and 152 ppm over DNL-6. The peaks at 198 ± 5, 188 ± 5 and 152 ppm can be assigned to polymethylbenzenium cation (polyMB$^+$).[7a,13] The peaks at 243 ± 2 and 154 ppm are responsible for ploymethylcyclopentadienium cation (polyMCP$^+$).[9,14] The ^{13}C NMR of pentamethylcyclopentadienium cation prepared in 98% H_2SO_4 and adsorbed on H-Beta are shown in Figure S9, which reconfirms the assignment. The signals from the saturated ring carbon atoms of polyMB$^+$ with chemical shift near 57 ppm are always overlapped by the signals from the surface methoxy groups.[15] The aforementioned two types of carbonium cations can be clearly detected over SAPO-34 and DNL-6 at 275 °C. Due to the very long induction period of SAPO-35 at 275 °C (>2 h, Figure 1), the reaction for the generation of carbenium cations in SAPO-35 is performed at 300 °C and polyMCP$^+$ and polyMB$^+$ are also detected. To the best of our knowledge, this is the first time to observe polyMCP$^+$ and polyMB$^+$ over SAPO-35 and SAPO-34 under real MTO reaction conditions.

The slight difference in chemical shift of carbonium cations may also result from the different number of the substituted methyl groups. However, it is very difficult to confirm the number of methyl groups on the carbenium cations only using solid-state NMR. Consequently, the materials confined in the cavities are further analyzed by GC-MS after dissolving the zeolite framework. These materials (Figure 3) are mainly methylbenzenes and adamantane hydrocarbons. More importantly, the neutral counterparts of polyMB$^+$ and polyMCP$^+$, polymethylmethylenecyclohexadiene (PMMC) and polymethylcyclopentadiene, are also detected (Figure 3 and S10).

Over SAPO-35, two isomers of trimethylcyclopentadiene (triMCP) (1,2,3-triMCP and 1,2,4-triMCP)[14b] and a small amount of tetramethylcyclopentadiene (tetraMCP) are clearly detected, but no pentamethylcyclopentadienes are observed. So the NMR signals at 242 and 154 ppm over SAPO-35 are responsible for the carbonium cations of triMCP and tetraMCP. Very interestingly, 1,5,6,6-tetraMMC (1,5,6,6-tetramethyl- 3-methylene-1,4-cyclohexdiene), the neutral counterparts of 1,2,2,3,5-pentaMB$^+$, is also detected with retention time between that of 1,2,4,5-tetraMB and pentaMB.[14b] The NMR signals at 203 and 195 ppm over SAPO-35 are assigned to 1,2,2,3,5-pentaMB$^+$.

Over SAPO-34, triMCP, tetraMCP, and pentaMCP isomers are all identified; however, PMMC can not be clearly

DOI: 10.1021/cs501669k
ACS Catal. 2015, 5, 661−665

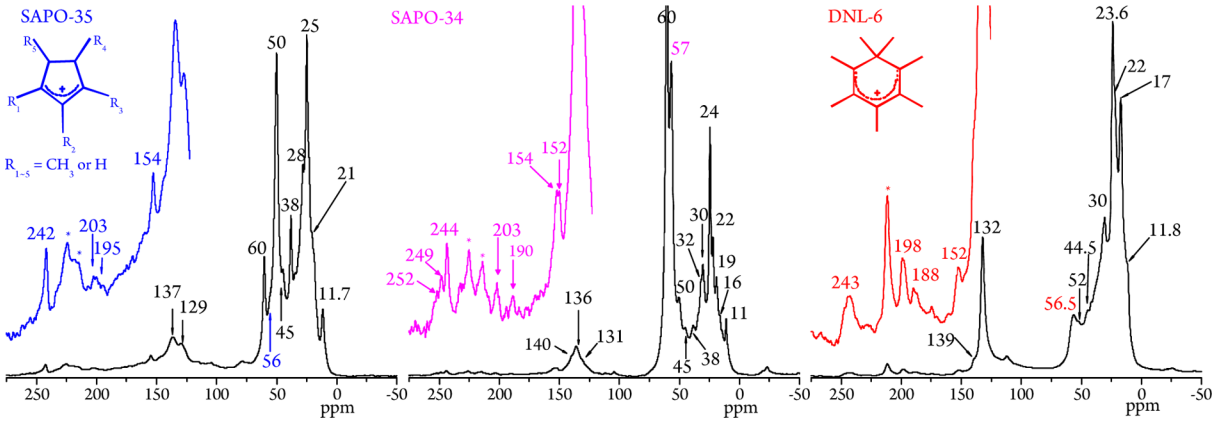

Figure 2. ^{13}C MAS NMR spectra of the catalysts after ^{13}C-methanol conversion for ~50 min at 275 °C (DNL-6 and SAPO-34) and 30 min at 300 °C for SAPO-35; * indicates the spinning sideband.

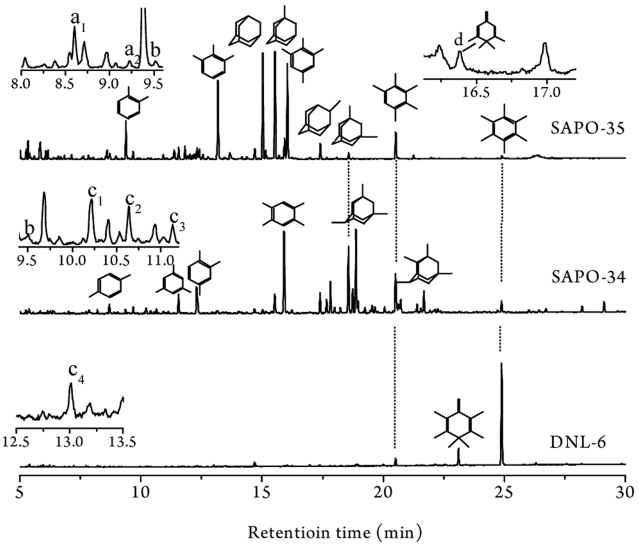

Figure 3. GC-MS chromatograms of the organic materials retained in the catalysts after methanol conversion, WHSV of MeOH = 2.0 h^{-1}, He/MeOH (in mol) =10, SAPO-34, and DNL-6 at 275 °C, SAPO-35 at 300 °C. *a_1 and a_2: triMCP; b: tetraMCP; c1, c2, c3 and c4: isomers of pentaMCP; d: tetraMMC (1,5,6,6-tetramethyl-3-methylene- 1,4-cyclohexdiene).

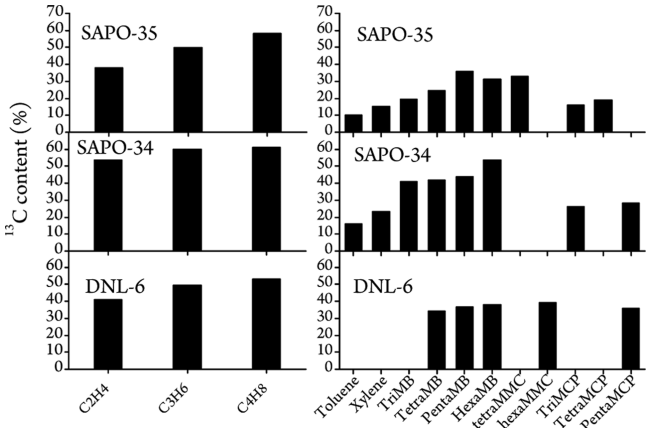

Figure 4. ^{13}C content of olefin products in the volatile phase (left) and confined species in the catalysts (right) of the ^{12}C/^{13}C switch experiments over SAPO-35 at 300 °C, SAPO-34 and DNL-6 at 275 °C.

distinguished. Over DNL-6, pentaMCP and hexamethylmethylenecyclohexadiene (hexaMMC) are clearly detected. The ex situ GC-MS results are well reconciled with the in situ solid-state NMR characterizations and demonstrate that the numbers of methyl groups on the carbenium cations vary with the cavity size.

Furthermore, 1,2,3-trimethylbenzene (triMB), 1,2,3,5-tetramethylbenzene (tetraMB), and pentamethylbenzene (pentaMB) are predominantly formed over SAPO-35, whereas 1,2,4,5-tetraMB and pentaMB are predominantly formed over SAPO-34. However, hexamethylbenzene (hexaMB) is the most predominant organics confined in DNL-6. This is consistent with the NMR spectra (Figure 2) especially in the range of 130−140 ppm which are assigned to alkylated aromatics.

To discriminate the active intermediates from the spectators, ^{12}C/^{13}C-methanol switch experiments are performed and the ^{13}C content of these species is employed as an indicator of the reactivity toward methanol conversion (Figure 4). As for SAPO-34 and DNL-6, the ^{13}C content of methylbenzenes increases with the number of methyl groups on benzene ring, which is consistent with the previous reports.[7a,8b,c] However, over SAPO-35, hexaMB exhibits lower ^{13}C content than pentaMB, whereas 1,5,6,6-tetraMMC shows comparable activity with the corresponding polymethylbenzene. This indicates that the steric constraint from the small *lev* cavities may depress the reactivity of hexaMB and make tetraMMC and pentaMB as the active intermediates. Detailed isotopomer distribution patterns of individual species are shown in Figure S11.

To further elucidate the confinement effects of cavity on carbenium cations, the theoretical calculations are also conducted using DFT-D2 method[16] at the GGA PBE[17] level with TNP basis set in Dmol^3 packages,[18] which has been proven to be an indispensable method to study the complicated MTO reactions.[7c,19]

First, the elementary steps of the methylation of tetraMB, pentaMB, and hexaMB to form the corresponding polymethylbenzenium cations are studied, and the intrinsic Gibbs free-energy barriers are shown in Figure 5. Over SAPO-34 and DNL-6, the predicted barriers decrease with the number of incorporated methyl groups. However, this trend does not keep over SAPO-35, where the barrier is largely enhanced when methyl groups increase to six. Detailed free energy profiles are plotted in Figure S12. Special attention should be paid to the

DOI: 10.1021/cs501669k
ACS Catal. 2015, 5, 661−665

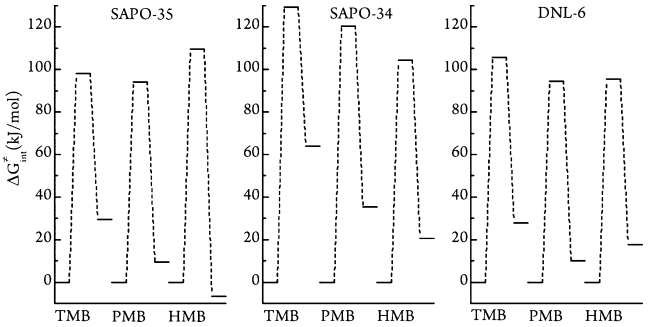

Figure 5. Intrinsic free-energy barriers (275 °C) of the methylation of tetraMB (TMB), pentaMB (PMB), and hexaMB (HMB) over SAPO-35, SAPO-34, and DNL-6.

energy increase after adsorption of pentaMB or hexaMB in methanol preadsorbed SAPO-35 and the energy decrease over SAPO-34 and DNL-6, which clearly shows the confinement and stabilization effects of the cavities.

The detailed transition-state (TS) geometries of hexaMB methylation (described in Figure S13−15) show that the *lev* cavity of SAPO-35 is excessively filled, the *cha* cavity of SAPO-34 is very appropriate, and the α cavity of DNL-6 is too large and still has void spaces. The length of the forming C−C bond for the TS in SAPO-35 is ∼0.1 Å longer than those in SAPO-34 and DNL-6 (Figure S14), which accompanies with severe deformation of the methyl groups on the benzene plane (Figure S15). These calculation results directly demonstrate the steric restriction of cavity on the transition-state of methylation reaction and provide a theoretic explanation of the prohibition of heptaMB$^+$ formation over SAPO-35, which are consistent with the results of in situ solid-state NMR characterization and the isotopic switch experiments.

Second, the stability of bulkier intermediates from which olefins may be split off[5b,c] are also considered and correlated to product selectivity. As shown in Figure S16, polymethylbenzenium cations with butyl side chain are stable in DNL-6, while polymethylbenzenium cations with shorter side chains (e.g., methyl and ethyl) are stable in SAPO-34. However, due to the steric constraints, heptaMB$^+$ and intermediates with longer side chain are not stable in SAPO-35. The smaller methylbenzenium (1,2,2,3,5-pentaMB$^+$) and methylcyclopentadienium cations (triMCP$^+$ and tetraMCP$^+$) could act as the active intermediates, from which ethene could be generated as the main product. This is in agreement with the product selectivity shown in Figure 1 and also consistent with the reports that the lower methylbenzenes over H-ZSM-5 might be responsible for ethene formation.[14b,20]

Moreover, the catalyst activity can also be correlated with the type of intermediates. Generally, hexaMB and heptaMB$^+$ are the most active hydrocarbon pool species. The reactions involving these intermediates are easy to proceed with lower barriers, which explain the high reactivity of SAPO-34 and DNL-6. Comparably, due to the steric restriction, MTO reaction over SAPO-35 has to proceed via other route permitted by the reaction environment, so lower catalyst activity is obtained (Figure1). The observation of polyMCP$^+$ and tetraMMC over SAPO-35 implies the former proposed paring mechanism,[21] involving ring contraction of aromatic intermediates and generation of polymethylcylcopentadienium cations, may be predominant. This is also supported by the isotopomer distributions of confined species (Figure S11). The distinct pathway following side-chain methylation mechanism,[22] which requires larger space for the methylation of exocyclic double bond of six-membered ring intermediates,[22] was proved to be the prevailing route over DNL-6.[7a]

In conclusion, two types of carbenium cations, polyMB$^+$ and polyMCP$^+$, are directly observed over SAPO molecular sieves with different cavities under real MTO reaction conditions. Their reactivity and role played in olefins generation are verified by isotopic tracing method and theoretical calculations. By careful comparison, it is concluded that the cavity size controls the molecular size and reactivity of confined species, which results in different MTO activity and product selectivity. The steric constraints imposed by the smaller cavities limit the formation and reactivity of bulky intermediates and result in higher ethene selectivity and lower methanol conversion. These findings are important for understanding the complicated MTO reaction mechanisms and designing new catalysts to improve product selectivity.

■ ASSOCIATED CONTENT

Supporting Information

The following file is available free of charge on the ACS Publications website at DOI: 10.1021/cs501669k.

Experimental details, catalyst characterization, enlarged part of GC-MS chromatograms of polymethylcyclopentadienium cations, and theoretical calculation details (PDF)

■ AUTHOR INFORMATION

Corresponding Author

*E-mail: liuzm@dicp.ac.cn. Fax: +86-411-84379335.

Notes

The authors declare no competing financial interest.

■ ACKNOWLEDGMENTS

We are very grateful for the financial support of the National Natural Science Foundation of China (No. 21273005, 21273230, 21103180).

■ REFERENCES

(1) Smit, B.; Maesen, T. L. M. *Nature* **2008**, *451*, 671−678.
(2) Anderson, M. W.; Klinowski, J. *Nature* **1989**, *339*, 200−203.
(3) (a) Dalian Institute of Chemical Physics, Chinese Academy of Sciences. http://english.dicp.cas.cn/rh/rp/201008/t20100811_57268.html (accessed Dec 24, 2014). (b) Liang, J.; Li, H. Y.; Zhao, S.; Guo, W. G.; Wang, R. H.; Ying, M. L. *Appl. Catal.* **1990**, *64*, 31−40. (c) Li, J.; Wei, Y.; Liu, G.; Qi, Y.; Tian, P.; Li, B.; He, Y.; Liu, Z. *Catal. Today* **2011**, *171*, 221−228.
(4) Olsbye, U.; Svelle, S.; Bjorgen, M.; Beato, P.; Janssens, T. V. W.; Joensen, F.; Bordiga, S.; Lillerud, K. P. *Angew. Chem., Int. Ed.* **2012**, *51*, 5810−5831.
(5) (a) Stocker, M. *Microporous Mesoporous Mater.* **1999**, *29*, 3−48. (b) Haw, J. F.; Song, W. G.; Marcus, D. M.; Nicholas, J. B. *Acc. Chem. Res.* **2003**, *36*, 317−326. (c) Cui, Z. M.; Liu, Q.; Song, W. G.; Wan, L. J. *Angew. Chem., Int. Ed.* **2006**, *45*, 6512−6515. (d) Wang, W.; Hunger, M. *Acc. Chem. Res.* **2008**, *41*, 895−904.
(6) Hereijgers, B. P. C.; Bleken, F.; Nilsen, M. H.; Svelle, S.; Lillerud, K. P.; Bjorgen, M.; Weckhuysen, B. M.; Olsbye, U. *J. Catal.* **2009**, *264*, 77−87.
(7) (a) Li, J.; Wei, Y.; Chen, J.; Tian, P.; Su, X.; Xu, S.; Qi, Y.; Wang, Q.; Zhou, Y.; He, Y.; Liu, Z. *J. Am. Chem. Soc.* **2012**, *134*, 836−839. (b) Wragg, D. S.; O'Brien, M. G.; Bleken, F. L.; Di Michiel, M.; Olsbye, U.; Fjellvag, H. *Angew. Chem., Int. Ed.* **2012**, *51*, 7956−7959. (c) Lesthaeghe, D.; De Sterck, B.; Van Speybroeck, V.; Marin, G. B.;

DOI: 10.1021/cs501669k
ACS Catal. 2015, 5, 661−665

Waroquier, M. *Angew. Chem., Int. Ed.* **2007**, *46*, 1311−1314. (d) Arstad, B.; Kolboe, S. *J. Am. Chem. Soc.* **2001**, *123*, 8137−8138. (e) McCann, D. M.; Lesthaeghe, D.; Kletnieks, P. W.; Guenther, D. R.; Hayman, M. J.; Van Speybroeck, V.; Waroquier, M.; Haw, J. F. *Angew. Chem., Int. Ed.* **2008**, *47*, 5179−5182. (f) Yamazaki, H.; Shima, H.; Imai, H.; Yokoi, T.; Tatsumi, T.; Kondo, J. N. *Angew. Chem., Int. Ed.* **2011**, *50*, 1853−1856. (g) Bhawe, Y.; Moliner-Marin, M.; Lunn, J. D.; Liu, Y.; Malek, A.; Davis, M. *ACS Catal.* **2012**, *2*, 2490−2495.

(8) (a) Nicholas, J. B.; Haw, J. F. *J. Am. Chem. Soc.* **1998**, *120*, 11804−11805. (b) Song, W. G.; Haw, J. F.; Nicholas, J. B.; Heneghan, C. S. *J. Am. Chem. Soc.* **2000**, *122*, 10726−10727. (c) Bjorgen, M.; Bonino, F.; Kolboe, S.; Lillerud, K. P.; Zecchina, A.; Bordiga, S. *J. Am. Chem. Soc.* **2003**, *125*, 15863−15868. (d) Dahl, I. M.; Kolboe, S. *J. Catal.* **1994**, *149*, 458−464. (e) Dahl, I. M.; Kolboe, S. *J. Catal.* **1996**, *161*, 304−309.

(9) Xu, S. T.; Zheng, A. M.; Wei, Y. X.; Chen, J. R.; Li, J. Z.; Chu, Y. Y.; Zhang, M. Z.; Wang, Q. Y.; Zhou, Y.; Wang, J. B.; Deng, F.; Liu, Z. M. *Angew. Chem., Int. Ed.* **2013**, *52*, 11564−11568.

(10) Wei, Y.; Li, J.; Yuan, C.; Xu, S.; Zhou, Y.; Chen, J.; Wang, Q.; Zhang, Q.; Liu, Z. *Chem. Commun.* **2012**, *48*, 3082−3084.

(11) Wang, W.; Jiang, Y. J.; Hunger, M. *Catal. Today* **2006**, *113*, 102−114.

(12) Salehirad, F.; Anderson, M. W. *J. Catal.* **1996**, *164*, 301−314.

(13) Song, W. G.; Nicholas, J. B.; Sassi, A.; Haw, J. F. *Catal. Lett.* **2002**, *81*, 49−53.

(14) (a) Song, W. G.; Nicholas, J. B.; Haw, J. F. *J. Phys. Chem. B* **2001**, *105*, 4317−4323. (b) Wang, C.; Chu, Y.; Zheng, A.; Xu, J.; Wang, Q.; Gao, P.; Qi, G.; Gong, Y.; Deng, F. *Chem. -Eur. J.* **2014**, *20*, 12432−12443.

(15) Li, J.; Wei, Y.; Xu, S.; Tian, P.; Chen, J.; Liu, Z. *Catal. Today* **2014**, *226*, 47−51.

(16) Grimme, S. *J. Comput. Chem.* **2006**, *27*, 1787−1799.

(17) Perdew, J. P.; Burke, K.; Ernzerhof, M. *Phys. Rev. Lett.* **1996**, *77*, 3865−3868.

(18) (a) Delley, B. *J. Chem. Phys.* **1990**, *92*, 508−517. (b) Delley, B. *J. Chem. Phys.* **2000**, *113*, 7756−7764. (c) *Materials Studio*, version 6.0; Accelrys Inc.: San Diego, 2011.

(19) (a) Clark, L. A.; Sierka, M.; Sauer, J. *J. Am. Chem. Soc.* **2004**, *126*, 936−947. (b) Svelle, S.; Tuma, C.; Rozanska, X.; Kerber, T.; Sauer, J. *J. Am. Chem. Soc.* **2009**, *131*, 816−825. (c) Van Speybroeck, V.; Van der Mynsbrugge, J.; Vandichel, M.; Hemelsoet, K.; Lesthaeghe, D.; Ghysels, A.; Marin, G. B.; Waroquier, M. *J. Am. Chem. Soc.* **2011**, *133*, 888−899.

(20) Svelle, S.; Joensen, F.; Nerlov, J.; Olsbye, U.; Lillerud, K. P.; Kolboe, S.; Bjorgen, M. *J. Am. Chem. Soc.* **2006**, *128*, 14770−14771.

(21) (a) Bjorgen, M.; Olsbye, U.; Petersen, D.; Kolboe, S. *J. Catal.* **2004**, *221*, 1−10. (b) Arstad, B.; Kolboe, S.; Swang, O. *J. Phys. Chem. A* **2005**, *109*, 8914−8922. (c) Bjorgen, M.; Akyalcin, S.; Olsbye, U.; Benard, S.; Kolboe, S.; Svelle, S. *J. Catal.* **2010**, *275*, 170−180.

(22) (a) Sassi, A.; Wildman, M. A.; Ahn, H. J.; Prasad, P.; Nicholas, J. B.; Haw, J. F. *J. Phys. Chem. B* **2002**, *106*, 2294−2303. (b) Sassi, A.; Wildman, M. A.; Haw, J. F. *J. Phys. Chem. B* **2002**, *106*, 8768−8773. (c) Arstad, B.; Nicholas, J. B.; Haw, J. F. *J. Am. Chem. Soc.* **2004**, *126*, 2991−3001.

DOI: 10.1021/cs501669k
ACS Catal. 2015, 5, 661−665